KSOE

Journal of Ocean Engineering and Technology 38(2), 53-63, April, 2024
https://doi.org/10.26748/KSOE.2024.046

pISSN 1225-0767
eISSN 2287-6715

Original Research Article

Optimization Analysis of the Shape and Position of a Submerged Breakwater for Improving Floating Body Stability

Sanghwan Heo[1,3], Weoncheol Koo[2] and MooHyun Kim[4]

[1]*Research Associate, Department of Naval Architecture and Ocean Engineering, Inha University, Incheon, Korea*
[2]*Professor, Department of Naval Architecture and Ocean Engineering, Inha University, Incheon, Korea*
[3]*Visiting Scholar, Department of Ocean Engineering, Texas A&M University, USA*
[4]*Professor, Department of Ocean Engineering, Texas A&M University, USA*

KEYWORDS: Submerged breakwater, Hydrodynamics, Frequency-domain boundary element method, Optimization analysis, Particle swarm optimization

ABSTRACT: *Submerged breakwaters can be installed underneath floating structures to reduce the external wave loads acting on the structure. The objective of this study was to establish an optimization analysis framework to determine the corresponding shape and position of the submerged breakwater that can minimize or maximize the external forces acting on the floating structure. A two-dimensional frequency-domain boundary element method (FD-BEM) based on the linear potential theory was developed to perform the hydrodynamic analysis. A metaheuristic algorithm, the advanced particle swarm optimization, was newly coupled to the FD-BEM to perform the optimization analysis. The optimization analysis process was performed by calling FD-BEM for each generation, performing a numerical analysis of the design variables of each particle, and updating the design variables using the collected results. The results of the optimization analysis showed that the height of the submerged breakwater has a significant effect on the surface piercing body and that there is a specific area and position with an optimal value. In this study, the optimal values of the shape and position of a single submerged breakwater were determined and analyzed so that the external force acting on a surface piercing body was minimum or maximum.*

1. Introduction

With the increasing demand for industrial and residential land, studies have been conducted on the construction of very large floating structures, such as floating airports, floating bridges, and multipurpose marine spaces, by installing floating structures in coastal and offshore areas (Watanabe et al., 2004; Lamas-Pardo et al., 2015). The first step in the design of such floating structures is to conduct a hydrodynamic analysis considering wave loads (Tavana and Khanjani, 2013). To reduce the hydroelastic responses of floating structures, various methods have been presented, including submerged breakwaters, floating breakwaters, and oscillating water column chambers. Among them, submerged breakwaters are the most effective structures (Wang et al., 2010). The main purpose of submerged breakwaters is to increase reflected waves and dissipate the wave energy or reduce the energy of transmitted waves (Huang et al., 2003) for reducing the wave loads acting on floating structures.

Two-dimensional (2D) domain analysis is mainly conducted in studies on submerged breakwaters because breakwaters are installed parallel to the shoreline and have a constant cross-section with a long shape. Studies have been actively conducted to analyze the changes in water surface caused by submerged breakwaters. Koley et al. (2020) conducted an experiment and boundary element method (BEM)-based numerical analysis on permeable rubble mound breakwaters. They conducted a parametric study on the shape of breakwaters and analyzed its effects on reflection, dissipation, and transmission coefficients. Jeong et al. (2021) analyzed the change in the transmission coefficient of submerged breakwaters composed of tetrapods using the environmental conditions of the coast of Korea, empirical formulas, and a wave deformation model (WADEM). Khan et al. (2021) analyzed the reflection and dissipation of incident waves caused by multi-layered trapezoidal porous rubble mound breakwaters using the multi-domain boundary element method (MDBEM). Loukili et al. (2021) analyzed the change in the reflection and transmission

Received 6 February 2024, revised 18 February 2024, accepted 25 February 2024
Corresponding author Weoncheol Koo: +82-32-860-7348, wckoo@inha.ac.kr

coefficients caused by a single rectangular submerged breakwater using the meshless singular boundary method. Ni and Teng (2021a; 2021b) analyzed the reflection coefficient of the porous rectangular and trapezoidal submerged breakwaters installed on a permeable inclined seabed using a modified mild-slope equation. They conducted a parametric analysis of the Bragg resonance caused by the porosity, the number and height of breakwaters, the distance between breakwaters, and the slope of the seabed. Patil and Karmakar (2021) conducted a parametric analysis of the reflection and transmission coefficients of impermeable and permeable submerged breakwaters in various shapes using MDBEM. These numerical analysis studies were conducted in the frequency domain. Time-domain numerical analysis and experimental studies have also been actively conducted. Lee et al. (2019) conducted an experimental study on tide-adapting submerged breakwaters and reported that their wave-breaking performance is superior to that of ordinary submerged breakwaters. Lee et al. (2002) conducted an experimental and numerical study on the distribution of vorticity, turbulence, and wave height according to the density, width, and arrangement of submerged rigid vegetation. Min et al. (2023) analyzed the reflection, transmission, and dissipation coefficients of dual submerged breakwaters using a fully nonlinear numerical wave tank (NWT) based on the boundary element method considering porous domain. They also conducted an analysis of the change in wave height caused by breakwaters and the pressure distribution inside permeable submerged breakwaters.

Studies have been actively conducted considering the interaction between submerged breakwaters and rear structures in the 2D domain. Their main purpose was to reduce the wave load acting on the structures by increasing reflected waves or dissipating the wave energy through the change in flow field caused by submerged breakwaters. Manisha et al. (2019) analyzed the reflected waves and the reduction in the wave load acting on floating bridges caused by various shapes of submerged breakwaters or trenches. Vijay et al. (2021) conducted a parametric analysis of reflection and transmission coefficients and the external forces acting on floating docks considering the interaction between submerged breakwaters in various shapes and fixed floating docks. Jiang et al. (2022) analyzed the reflection, dissipation, and enhancement coefficients by double and triple submerged breakwaters using the volume-averaged Reynolds-averaged Navier–Stokes equation (VARANS). They also analyzed the effect of submerged breakwaters on the external forces acting on a vertical breakwater, and reported that triple submerged breakwaters with high porosity most efficiently reduce the wave external force acting on the rear structure.

The design of submerged breakwaters for the reduction in wave loads acting on floating bodies and their dynamic stability involves numerous design variables, such as the distance between the floating body and breakwaters and the shape of breakwaters. To analyze the optimization problem for these design variables, metaheuristic algorithms that can effectively find the maximum or minimum value based on the objective function are used. Metaheuristic algorithms can be classified into evolutionary algorithms, swarm-based algorithms, physics-based algorithms, and human-based algorithms (Kaveh and Mesgari, 2023). Metaheuristic algorithms are also widely used in the field of ocean engineering. Zhu et al. (2022) conducted an optimization analysis of the layout of wave energy converters using artificial neural networks and adaptive genetic algorithms. Ferri and Marino (2023) conducted an optimization analysis of substructures for 10 MW-class floating offshore wind turbines using genetic algorithms. Gandomi et al. (2023) analyzed the reflection and transmission coefficients of by permeable breakwaters using the conditional value-at-risk method (CvaR) based on the multilayer perceptron neural network and second-generation nondominated sorting genetic algorithm (NSGA-II). Jeong and Koo (2023) conducted an optimization analysis of the power output of wave energy converters using the three-dimensional frequency-domain boundary element method (FD-BEM) based on the potential flow theory. They compared the optimization analysis results for genetic algorithms, simulated annealing, particle swarm optimization (PSO), and advanced PSO (Chen et al., 2018), and described the superiority of advanced PSO. Zhang et al. (2023) conducted an optimization analysis of the structural parameters of articulated offshore wind turbines using the third-generation nondominated sorting genetic algorithm (NSGA-III).

This study aimed to construct an optimization analysis framework to determine the optimal values for the shape and position of submerged breakwaters that can minimize or maximize the external forces acting on the floating structure to improve its stability. To conduct a hydrodynamic analysis considering the interaction between the floating structure and the submerged breakwaters, a 2D FD-BEM program based on the linear potential theory was developed. It was coupled with a metaheuristic algorithm to conduct the optimization analysis. To the best of our knowledge, the development of a linked analysis framework of NWT and an optimization algorithm that can analyze the 2D hydrodynamic problems considering various sea bottoms was attempted for the first time. As a metaheuristic algorithm, the advanced PSO proposed by Chen et al., (2018) and demonstrated superiority by Jeong and Koo (2023) was used in this study. The optimization analysis is performed by calling FD-BEM for each generation, conducting a numerical analysis of the design variables of each particle, and updating the design variables using the collected results. In this study, the optimal values for the shape and position of a single submerged breakwater that minimize or maximize the external forces acting on a fixed surface piercing body were determined and analyzed.

2. Mathematical Formulation

Fig. 1 shows the linked analysis framework of the FD-BEM program and optimization algorithm. The optimization algorithm sets the initial values of the design variable vectors corresponding to the number of particles using the ranges of the design variables entered by the user and the objective function. The opposition-based learning

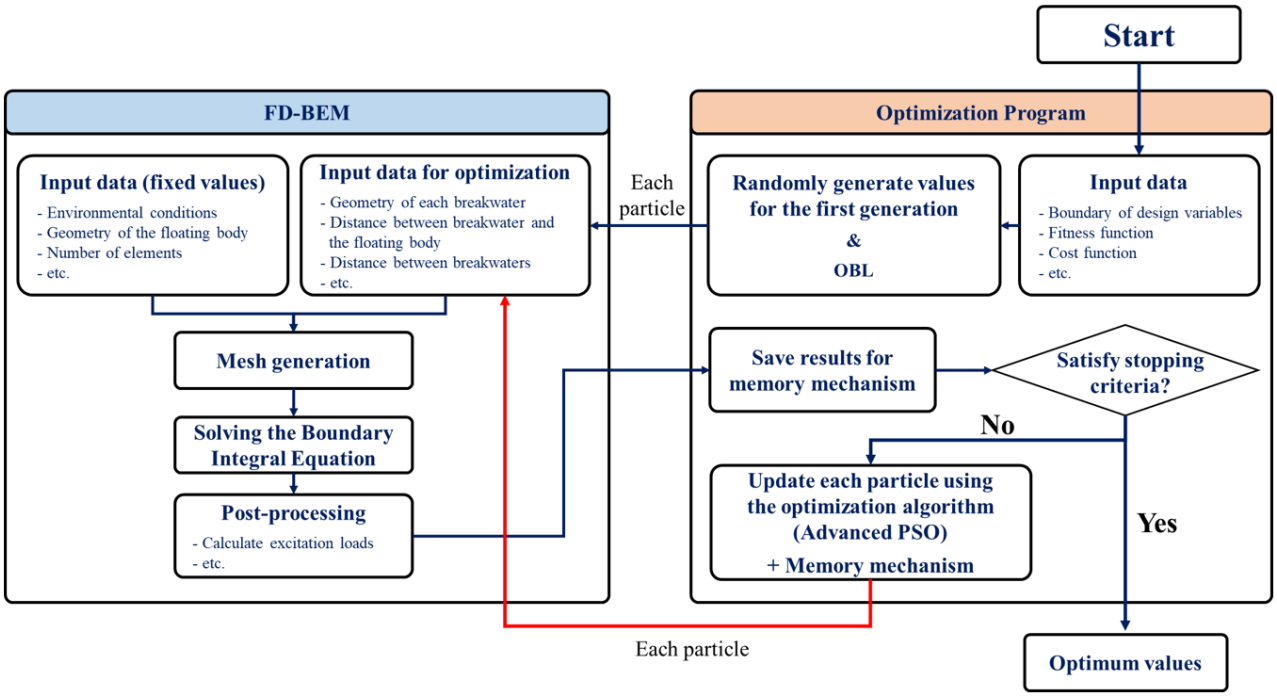

Fig. 1 Description of the linked analysis framework of the FD-BEM program and optimization algorithm

technique is applied to determine the particles of the first generation (Ahandani, 2016). The FD-BEM program is executed using the design variables of each particle, and the objective function is calculated using the output values. The design variables used for computation are stored in memory, and the analysis time can be reduced by preventing the execution of the same calculation. If the objective function satisfies the stopping criteria or the maximum number of iteration, the entire computation is terminated, and the design variable vectors are defined as the optimal values.

2.1 FD-BEM

This study employed a numerical analysis technique (boundary element method) based on the linear potential theory in which the fluid in the computational domain has inviscid, irrotational, and incompressible characteristics to calculate 2D hydrodynamic problems. The governing equation of the computational domain is the Laplace equation, which can be expressed using the velocity potential as follows.

$$\nabla^2\phi = 0 \tag{1}$$

In hydrodynamic problems of general floating bodies, the velocity potential is the sum of the incident, diffraction, and radiation velocity potentials. In this study, it was assumed that the motion of the floating body was fixed, and the effect of the radiated wave was not considered as shown in Eq. (2). The incident wave was assumed to be a linear wave, and the incident velocity potential can be calculated using Eq. (3).

$$\phi = \phi_I + \phi_D \tag{2}$$

$$\phi_I = -i\frac{gH}{2\omega}\frac{\cosh k(z+h)}{\cosh kh}e^{ikx} \tag{3}$$

where ϕ_I and ϕ_D are the velocity potentials of the incident and radiation, respectively. g is the gravitational acceleration, H is the wave height, ω is the frequency of the incident wave, k is the wavenumber, and h is the water depth. x is the horizontal coordinate in the incident wave direction, and z is the vertical displacement from the water surface.

The boundary integral equation can be obtained using Green's function, which is the fundamental solution of the Laplace equation, and Green's second identity as follows.

$$\frac{1}{2}\phi + \int_\Gamma \left(\phi\frac{\partial G}{\partial \boldsymbol{n}}\right)d\Gamma = \int_\Gamma \left(G\frac{\partial \phi}{\partial \boldsymbol{n}}\right)d\Gamma \tag{4}$$

where $G = 1/(2\pi)\cdot ln(1/r)$ is the 2D Green's function, and r is the distance between the source and field points. Γ is the boundary of the computational domain, and $\boldsymbol{n}$ is the normal vector at the boundary. Fig. 2 shows the computational domain for conducting the hydrodynamic numerical analysis considering the interaction between a floating body and a submerged breakwater. To solve Eq. (4), the following boundary conditions were applied to the computational domain.

(1) Free surface boundary conditions

The dynamic and kinematic free surface boundary conditions in the frequency domain may be integrated as follows.

$$\frac{\partial \phi}{\partial \boldsymbol{n}} - \frac{\omega^2}{g}\phi = 0 \quad on\ \Gamma_{Free} \tag{5}$$

(2) Radiation boundary conditions

The Sommerfeld radiation boundary condition was used to implement the open sea condition. The boundary condition (Eq. (6)) that considers the influence of the incident wave was applied to Γ_{Rad1} (Koley et al., 2020).

$$\frac{\partial(\phi-\phi_I)}{\partial \boldsymbol{n}}-ik(\phi-\phi_I)=0 \quad on\ \Gamma_{Rad1} \tag{6}$$

$$\frac{\partial \phi}{\partial \boldsymbol{n}}-ik\phi=0 \quad on\ \Gamma_{Rad2} \tag{7}$$

(3) Sea bottom and submerged breakwater boundary conditions

Non-penetration boundary conditions in which fluid particles cannot pass through the boundary were applied to the sea bottom and the submerged breakwater.

$$\frac{\partial \phi}{\partial \boldsymbol{n}}=0 \quad on\ \Gamma_{Bot} \text{ and } \Gamma_{BW}. \tag{8}$$

(4) Floating body boundary conditions

In this study, it was assumed that the motion of the floating body was fixed, and the external force acting on the floating body was calculated by solving only the diffraction problem without solving the radiation problem. The floating body boundary condition for solving the diffraction problem is as follows.

$$\frac{\partial \phi_D}{\partial \boldsymbol{n}}=-\frac{\partial \phi_I}{\partial \boldsymbol{n}} \quad on\ \Gamma_{FB} \text{ (for the diffractionproblem)} \tag{9}$$

The velocity potentials at all boundaries can be obtained by substituting Eqs. (5)–(9) into Eq. (4) and performing matrix operations through discretization.

The reflection and transmission coefficients at the open sea boundaries can be calculated using the velocity potentials at each radiation boundary (Vijay et al., 2021).

$$K_R=\left|\frac{i\omega}{gAN_0^2}\left[\int_{-h}^{0}\phi|_{Rad1}\,Z_0(z)dz\right]-1\right| \tag{10}$$

$$K_T=\left|\frac{i\omega}{gAN_0^2}\left[\int_{-h}^{0}\phi|_{Rad2}\,Z_0(z)dz\right]\right| \tag{11}$$

where K_R and K_T are the reflection and transmission coefficients, respectively. $Z_0(z)=\cosh k(z+h)/\cosh kh$ is the vertical eigenfunction, i.e., $N_0^2=\int_{-h}^{0}Z_0^2(z)dz$. As there is no wave energy loss, the total energy of the reflected and transmitted waves has a constant value ($K_R^2+K_T^2=1$).

The wave load acting on the floating body can be obtained by integrating the hydrodynamic pressure acting on the submerged surface, and the pressure acting on each element can be calculated using the Bernoulli equation.

$$\boldsymbol{F}=i\rho\omega\int\phi\boldsymbol{n}\,d\Gamma_{FB} \tag{12}$$

$$\boldsymbol{M}=i\rho\omega\int\phi(r_{xg}n_z-r_{zg}n_x)d\Gamma_{FB} \tag{13}$$

where $\boldsymbol{F}$ and $\boldsymbol{M}$ are the external force and moment vectors acting on the floating body, respectively. ρ is the density of the fluid, and r_{xg} and r_{zg} are the horizontal and vertical distances from the center of gravity of the floating body to each element, respectively. The external force components obtained through the frequency-domain analysis can be nondimensionalized as follows.

$$K_F=\frac{|\boldsymbol{F}|}{\rho gHh} \tag{14}$$

$$K_M=\frac{|\boldsymbol{M}|}{\rho gHh^2} \tag{15}$$

2.2 Metaheuristic Algorithm

Metaheuristic algorithms are representative optimization algorithms that are used to find the maximum or minimum values based on the

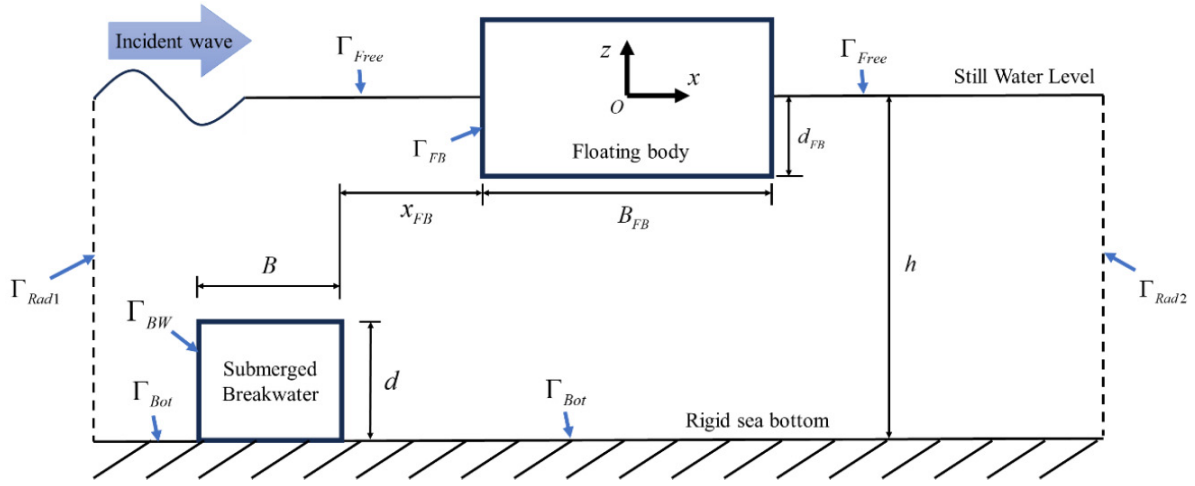

Fig. 2 Illustration of the computational domain and boundaries for a surface piercing body and submerged breakwater

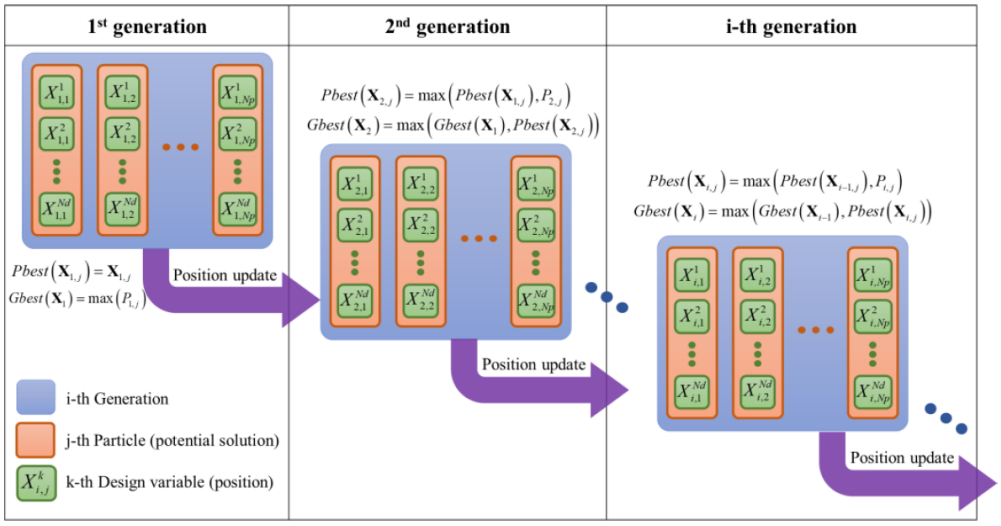

Fig. 3 Illustration of the procedure of the general PSO

objective function in optimization problems with multiple design variables. In this study, advanced PSO, one of a swarm-based algorithms, was applied for the optimization analysis (Eberhart and Kennedy, 1995; Shi and Eberhart, 1998; Chen et al., 2018). Jeong and Koo (2023) verified the superior performance of advanced PSO through the comparison and analysis of various metaheuristic algorithms.

Fig. 3 shows the procedure of the general PSO. Advanced PSO is composed of *Np* particles for each generation (iteration). Each particle is composed of *Nd* design variables, and the solution obtained from these design variables becomes the value of each particle. As the design variables converge from randomly generated initial values to the optimal values, particles can be said to be potential solutions. The value of each design variable in one particle is referred to as a position, which is updated by calculating the relative velocity between the particle and other particles for each generation. The velocity of the *k*-th design variable of the *j*-th particle in the *i*-th generation can be calculated as follows.

$$V_{i,j}^{k} = \alpha V_{i-1,j}^{k} + c_1\, rand_1 \left(Pbest(X_{i-1,j}^{k}) - X_{i-1,j}^{k}\right) + c_2\, rand_2 \left(Gbest(X_{i-1}^{k}) - X_{i-1,j}^{k}\right) \tag{16}$$

where $rand$ is a random variable between 0 and 1. $V_{i,j}^{k}$ and $X_{i,j}^{k}$ are the velocity and position of each design variable, respectively, which can be expressed in the vector form ($\boldsymbol{V}_{i,j} = \left[V_{i,j}^{1} \;\; V_{i,j}^{2} \;\cdots\; V_{i,j}^{Nd}\right]^{T}$, $\boldsymbol{X}_{i,j} = \left[X_{i,j}^{1} \;\; X_{i,j}^{2} \;\cdots\; X_{i,j}^{Nd}\right]^{T}$). $Pbest(\boldsymbol{X}_{i-1,j})$ is the optimal position vector of the *j*-th particle until the previous generation, and $Gbest(\boldsymbol{X}_{i-1})$ is the optimal position vector among all the particles until the previous generation. α is the linearly decreasing inertia weight proposed by Shi and Eberhart (1998). PSO shows an excellent performance when the value of the inertia weight starts with a value close to 1 and linearly decreases to 0.4. Accordingly, the initial value ($\alpha_{\max}$) and final value ($\alpha_{\min}$) of the inertia weight were set to 0.8 and 0.4, respectively, and α can be calculated as follows.

$$\alpha = \alpha_{\max} - \frac{Iter_i}{Iter_{\max}}(\alpha_{\max} - \alpha_{\min}) \tag{17}$$

where $Iter_i$ is the *i*-th generation, and $Iter_{\max}$ is the maximum number of generations. c_1 and c_2 were calculated using sine cosine acceleration coefficients (Chen et al., 2018).

$$c_1 = \partial sin\left(\frac{\pi}{2}\left(1 - \frac{Iter_j}{Iter_{\max}}\right)\right) + \delta, \tag{18}$$

$$c_2 = \partial cos\left(\frac{\pi}{2}\left(1 - \frac{Iter_j}{Iter_{\max}}\right)\right) + \delta, \tag{19}$$

where the values of ∂ and δ were 2 and 0.5, respectively (Chen et al., 2018).

After calculating the velocity using Eq. (16), the position can be updated using the following equation.

$$X_{i,j}^{k} = X_{i-1,j}^{k} + V_{i,j}^{k}. \tag{20}$$

The opposition-based learning technique was applied to improve the performance of the initial random design variables of the first generation (Ahandani, 2016). The computation speed was improved by setting calculations to be omitted when there were previous calculation results for the same design variable vector by applying the memory mechanism (Cao et al., 2022).

3. Numerical Analysis and Results

3.1 Verification of the Computation Results of FD-BEM

Before conducting the optimization analysis, the numerical analysis results were compared with the results of previous studies to verify the

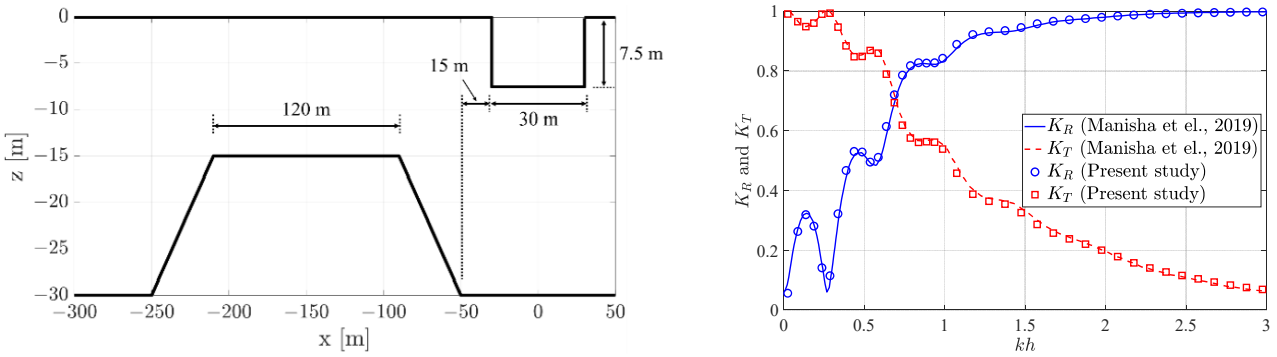

(a) (b)

Fig. 4 Comparison of reflection and transmission coefficients for a surface piercing body and a trapezoidal rigid submerged breakwater: (a) Calculation domain, (b) Reflection and transmission coefficients

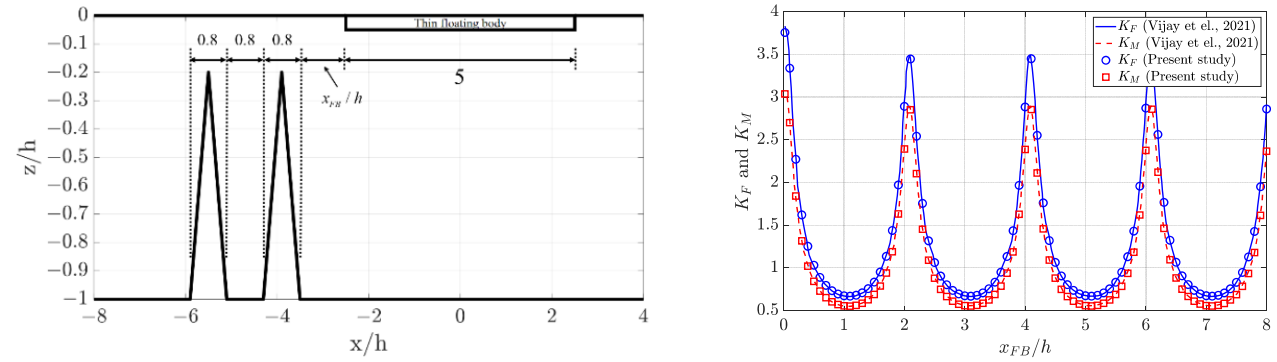

(a) (b)

Fig. 5 Comparison of external forces acting on a thin surface piercing body and two triangular rigid submerged breakwaters: (a) Calculation domain, (b) Vertical force and pitching moment

accuracy of the calculation of the developed 2D FD-BEM. Fig. 4(a) shows a surface piercing body and a trapezoidal rigid submerged breakwater. The width and draft of the structure are 60 and 7.5 m, respectively, and the water depth is 30 m. The lengths of the lower and upper sides of the breakwater are 200 and 120 m, respectively, and its height is 15 m. The distance between the structure and the breakwater is 15 m. Fig. 4(b) compares the reflection and transmission coefficients at the radiation boundary with the results of Manisha et al. (2019). The computation results of the present study were consistent with the results of the previous study, and the error was less than 3%.

Fig. 5(a) shows a thin surface piercing body and two triangular rigid submerged breakwaters. The width of the body is 5*h*, and its draft is very thin. For the two submerged breakwaters, the length of the lower side and the height are 0.8*h*. The distance between the breakwaters is 0.8*h*. Fig. 5(b) compares the vertical external force and pitching moment acting on the body with the results of Vijay et al. (2021) according to the distance between the surface piercing body and the breakwater. The computation results of the present study were consistent with the results of the previous study, and the error was less than 0.5%. Thus, it was determined that the developed FD-BEM program has sufficient accuracy to conduct a hydrodynamic analysis considering the interaction between the surface piercing body and the submerged breakwater.

3.2 Optimization Analysis of the Shape and Position of the Submerged Breakwater

3.2.1 Single submerged breakwater with a constant area

To examine the operational and computational performance of the developed linked analysis framework, the optimization analysis of the single submerged breakwater installed in front of the floating body and incident wave was conducted in the domain shown in Fig. 2. Motion response analysis must be conducted considering the radiated wave and mooring line caused by the floating body motion for evaluating the stability of the actual floating body. However, this study focused on the development of a computational procedure for the optimization analysis of the external forces acting on the floating body according to the shape and position of the submerged breakwater. Therefore, a situation in which the floating body is fixed was assumed. The limitations of this interpretation are that the radiated wave and its interaction with the submerged breakwater cannot be considered, and that the motion response of the floating body cannot be identified. However, the results of Fig. 5(b) show that the external force and pitching moment acting on the floating body have similar tendencies when the floating body is fixed, and accordingly, the total external force ($F_{Total} = \sqrt{F_x^2 + F_z^2}$) acting on the floating body according to the shape and position of the submerged breakwater was set as the objective function. In addition, the overturning moment caused by the

wave force acts on the actual submerged breakwater, and a stability analysis must be conducted considering it. However, as mentioned earlier, the overturning moment was not considered to focus on the development of a computation procedure for the optimization algorithm for the shape and position of the submerged breakwater.

In this study, structures with a width larger than the draft, such as floating docks, bridges, and airports, where stability is important, were assumed. The specifications of the floating body and the water depth (h) remained constant during the entire simulation process, and the width and draft of the floating body were 2h and 0.25h, respectively. The incident wave condition was the nondimensionalized wavenumber kh equal to 1.571 rad/s, and the wavelength of the incident wave was 4h. The distance between the floating body and the submerged breakwater (x_{FB}) and the height of the breakwater (d) were set as the design variables for conducting the optimization analysis. It was assumed that the installation cost of the breakwater (the area of the breakwater) was constant at one-tenth of the submerged area of the floating body ($A_{FB} = B_{FB} d_{FB}$), and the width of the breakwater is determined by its height. In this instance, the width of the breakwater can be calculated as follows.

$$A_{BW} = 0.1 A_{FB} \tag{21}$$

$$B = A_{BW}/d \tag{22}$$

where A_{BW} is the area of the submerged breakwater.

Table 1 presents the range of each design variable. x_{FB} ranged from 0.1h to 2h, and d ranged from 0.1h to various upper limits. The step size of the design variables was h/300, and the total number of possible simulations ranged from 17,701 ($0.1h \leq x_{FB}/h \leq 0.2h$) to 137,611 ($0.1h \leq x_{FB}/h \leq 0.9h$). The objective function was set so that the total external force acting on the floating body could be minimized or maximized, and optimization analysis was conducted for each case. The number of particles for the optimization analysis was set to 100 for all the cases, and the maximum number of generations (maximum iteration) was set to 500. Table 2 presents the configuration of the PC used for the optimization analysis. The analysis was conducted using the same PC for all the cases, and the time required for one simulation was two seconds or less.

Table 1 Boundaries of the design variables

Design variables	Lower limit	Upper limit	Step size
x_{FB}/h	0.1	2.0	1/300
d/h	0.1	0.2, 0.3, 0.4, 0.5, 0.6, 0.7, 0.8, 0.9	1/300

Table 2 PC configuration for simulation

Components	Description
CPU	Intel (R) Xeon (R) Platinum 8260 (2.40 GHz)
RAM	192 GB
OS	Windows 10

Table 3 presents the results of the optimization analysis conducted under the conditions of Table 1. At d/h = 0.9, the total analysis time was approximately 700 s, and approximately 1,200 simulations were performed. The design variables of the particles converged to the same values before 50 generations. The total external force acting on the floating body was nondimensionalized by dividing it by the external force in the absence of the submerged breakwater (F_{No}). In all the cases, the height of the breakwater converged to the largest value within the designated range. This is because the movement of fluid particles rapidly increases toward the water surface, and thus, an increase in the height of the breakwater has a significant influence on the fluid particles. Within the same installation cost (the area of the breakwater), an increase in the height of the breakwater within the permitted range has a significant influence on the floating body. In addition, it was confirmed that the force acting on the floating body can be minimized or maximized depending on the position of the submerged breakwater despite the same breakwater shape. As the force acting on the breakwater and the resulting overturning moment were not considered in this study, the values converged to make the width of the breakwater very thin. Therefore, a detailed analysis is required considering the stability of the breakwater as well as the position and shape of the breakwater based on its installation purpose.

Table 3 Optimal values for minimizing and maximizing the external force according to the upper limit of breakwater height

Upper limit of d/h	Optimal values					
	Minimizing wave force			Maximizing wave force		
	x_{FB}/h	d/h	F_{Total}/F_{No}	x_{FB}/h	d/h	F_{Total}/F_{No}
0.2	1.477	0.2	0.9591	0.447	0.2	1.0526
0.3	1.513	0.3	0.9312	0.480	0.3	1.0909
0.4	1.517	0.4	0.8938	0.487	0.4	1.1452
0.5	1.510	0.5	0.8460	0.483	0.5	1.2202
0.6	1.497	0.6	0.7863	0.470	0.6	1.3234
0.7	1.470	0.7	0.7121	0.447	0.7	1.4692
0.8	1.427	0.8	0.6175	0.407	0.8	1.6903
0.9	1.367	0.9	0.4844	0.347	0.9	2.0910

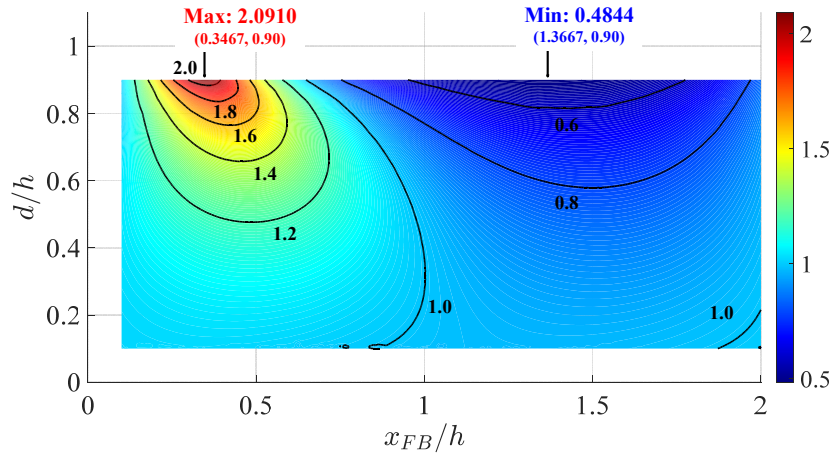

Fig. 6 Contour plot of the ratio of the external force acting on the floating body (values are interpolated)

Fig. 6 shows the contour plot of the ratio of the external force acting on the floating body obtained by conducting the optimization analysis. When x_{FB}/h was lower than approximately 0.6 (when the floating body and submerged breakwater were relatively close), the external force acting on the floating body increased regardless of the height of the breakwater. When it was higher than 1.0 (when the breakwater was relatively far away), the external force acting on the floating body decreased regardless of the height of the breakwater. As for the tendency of the external force, x_{FB}/h showed a tendency to decrease as the height of the breakwater increased when d/h was higher than 0.4 for both the minimum and maximum values. This is because the movement range of fluid particles increases toward the water surface, and thus, the position at which the fluid particles affect the interaction between the floating body and the breakwater also changes.

Fig. 7 compares the magnitude of the wave elevations according to the position of the submerged breakwater when d/h is 0.9. In Fig. 7(a), the black solid line indicates the wave elevation in the absence of the submerged breakwater. Standing waves were generated owing to the

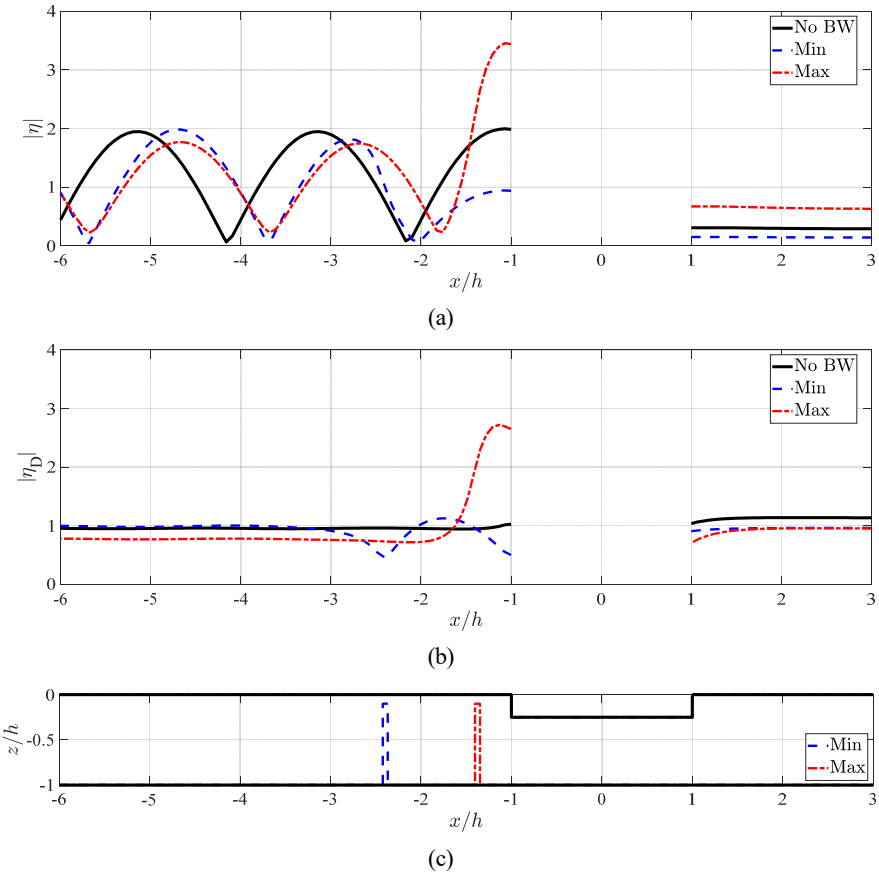

Fig. 7 Comparison of wave elevations according to the position of the submerged breakwater: (a) Total wave elevation, (b) Diffracted wave elevation, (c) Location of the floating body and breakwaters

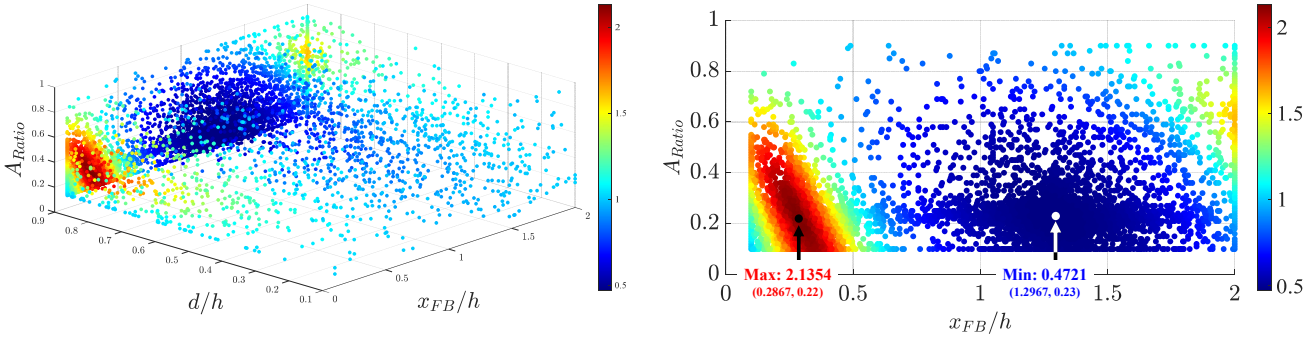

(a) (b)

Fig. 8 Scatter plot of the ratio of the external forces acting on the floating body according to x_{FB}/h, d/h, and A_{Ratio}; (a) Scatter plot for the three design variables, (b) Scatter plot at d/h=0.9

diffracted waves caused by the floating body. In the presence of the submerged breakwater, the wave elevation adjacent to the floating body differed by approximately 3.5 times depending on the position of the breakwater despite the same breakwater size. When the breakwater was close to the floating body, very large diffracted waves were generated and the magnitude of transmitted waves also increased, thereby increasing the external force acting on the floating body. When the breakwater was moved away by a certain distance from the floating body, both the reflected and transmitted waves were reduced by the destructive interference of the incident and diffracted waves, thereby decreasing the external force acting on the floating body.

3.2.2 Single submerged breakwater with various areas

An optimization analysis was conducted considering the area ratio between the submerged breakwater and the floating body as an additional design variable, and the area of the breakwater according to the area ratio was calculated using the following equation.

$$A_{BW} = A_{Ratio} A_{FB}, \tag{23}$$

where A_{Ratio} is the area ratio between the submerged breakwater and the floating body. It was set to range from 0.1 to 0.9 at a step size of 0.01. The total number of possible simulations is approximately 11 million (137,611×81), and the same values as in Section 3.2.1 were used for the objective function, the number of particles, and the maximum number of generations. The total analysis time was approximately 5,200 s, and approximately 7,500 simulations were performed. The design variables of the particles converged to the same values before 150 generations.

Fig. 8(a) shows the optimization analysis results for each design variable in a scatter plot. Dots are concentrated at d/h = 0.9. This is because the particles converged to the value when d/h was 0.9 as optimization calculations were repeated. Fig. 8(b) shows the results at d/h = 0.9. The case in which the ratio of the external forces acting on the floating body was increased by the breakwater (F_{Total}/F_{No}>1.0) mostly occurred when x_{FB}/h was lower than 0.5, and the x_{FB} value that maximized the ratio of the external force decreased as the area ratio increased. The values of x_{FB} that maximized and minimized the ratio of the external force differed by approximately one-fourth of the wavelength ($1h$), which indicates that the wavelength of the incident wave and the ratio of the external force are closely related. Based on the results of the ratio of the external force for the area ratio of the breakwater and x_{FB}/h, a large external force can be expected when d/h is 0.9, the area ratio is 0.22, and x_{FB}/h is 2.3. The ratio of the external force obtained by conducting a numerical analysis using these values was 2.0177, confirming that a large value occurred.

Note that a large area of the submerged breakwater is not necessarily good, and there is a specific position that has the optimal value. This indicates that an optimization analysis that considers various design variables is essential for detailed interpretation. It can also reduce the total analysis time to determine the optimal values because the objective function rapidly converges by preventing unnecessary simulation even if the number of simulation cases increases owing to the increased design variables.

4. Conclusion

In this study, a 2D FD-BEM was developed based on the linear potential theory and boundary element method, and it was coupled with advanced PSO, one of the metaheuristic algorithms, to construct an optimization analysis framework. For the first time, this study attempted to develop a linked analysis framework of a 2D NWT and an optimization algorithm that considers various sea bottoms. The FD-BEM proved the accuracy of the solution through a comparison with the results of previous studies, and advanced PSO is an algorithm with proven superiority. The execution of the FD-BEM program is automatically repeated using the design variable vectors generated in the optimization algorithm process. When the numerical analysis for each particle was finished, a memory mechanism was applied to prevent unnecessary calculations by storing the results in memory. Each design variable vector updates its position value by calculating the relative velocity with the optimal value, and the position value

continues to be updated over generations until the stopping criteria are satisfied.

To examine the operational and computational performance of the developed optimization analysis framework, an optimization analysis was conducted for the height and area of a single rigid submerged breakwater installed in front of a fixed floating body and an incident wave. The optimization analysis confirmed that the height of the submerged breakwater has a significant influence on the floating body, and that there is an optimal position for the breakwater. In addition, even if the number of simulation cases increased, the total analysis time to determine the optimal values could be reduced by preventing unnecessary simulation through the optimization analysis.

The developed 2D FD-BEM has limitations in considering the effects of nonlinearity, viscosity, and turbulence because it is based on the linear potential theory. However, it has sufficient precision to analyze reflected and transmitted waves and the external forces acting on floating bodies when a numerical analysis is conducted on long submerged and floating bodies. It is also suitable for conducting an optimization analysis that requires a large amount of simulation owing to the shorter analysis time compared with that of nonlinear analysis and computational-fluid-dynamics-based (CFD-based) analysis. As this study focused on developing an optimization analysis framework for the specifications of floating bodies and submerged breakwaters, the fixed floating body condition was applied. This has limitations in considering the interaction between the radiated waves caused by the floating body motion and the submerged breakwater. To overcome this, the precision of optimization analysis will be examined in follow-up studies through the motion response analysis of a floating body, including the mooring line, and a comparison with experiment results. In the future, various metaheuristic algorithms will be applied to the developed framework, and it will be expanded to time-domain analysis. Based on this, a hydrodynamic optimization analysis will be conducted on various ocean engineering problems.

Conflict of Interest

MooHyun Kim and Weoncheol Koo serve as editorial board members of the Journal of Ocean Engineering and Technology, but they had no role in the decision to publish this article. No potential conflict of interest relevant to this article was reported.

Funding

This study was supported by the MOTIE (Ministry of Trade, Industry, and Energy) in Korea, under the Human Resource Development Program for Industrial Innovation (Global) (P0017303, Smart Manufacturing Global Talent Training Program) supervised by the Korea Institute for Advancement of Technology (KIAT). This study was also supported by the National Research Foundation of Korea (NRF) grant funded by the Korea government (MSIT) (RS-2023-00278157).

References

Ahandani, M. A. (2016). Opposition-based learning in the shuffled bidirectional differential evolution algorithm. *Swarm and Evolutionary Computation*, *26*, 64−85. https://doi.org/10.1016/j.swevo.2015.08.002

Cao, F., Han, M., Shi, H., Li, M., & Liu, Z. (2022). Comparative study on metaheuristic algorithms for optimising wave energy converters. *Ocean Engineering*, *247*, 110461. https://doi.org/10.1016/j.oceaneng.2021.110461

Chen, K., Zhou, F., Yin, L., Wang, S., Wang, Y., & Wan, F. (2018). A hybrid particle swarm optimizer with sine cosine acceleration coefficients. *Information Sciences*, *422*, 218−241. https://doi.org/10.1016/j.ins.2017.09.015

Eberhart, R., & Kennedy, J. (1995, October). A new optimizer using particle swarm theory. In *MHS'95. Proceedings of the sixth international symposium on micro machine and human science, Nagoya, Japan* (pp. 39−43). IEEE. https://doi.org/10.1109/MHS.1995.494215

Ferri, G., & Marino, E. (2023). Site-specific optimizations of a 10 MW floating offshore wind turbine for the Mediterranean Sea. *Renewable Energy*, *202*, 921−941. https://doi.org/10.1016/j.renene.2022.11.116

Gandomi, M., Pirooz, M. D., Nematollahi, B., Nikoo, M. R., Varjavand, I., Etri, T., & Gandomi, A. H. (2023). Multi-criteria decision-making optimization model for permeable breakwaters characterization. *Ocean Engineering*, *280*, 114447. https://doi.org/10.1016/j.oceaneng.2023.114447

Huang, C. J., Chang, H. H., & Hwung, H. H. (2003). Structural permeability effects on the interaction of a solitary wave and a submerged breakwater. *Coastal engineering*, *49*(1−2), 1−24. https://doi.org/10.1016/S0378-3839(03)00034-6.

Jeong, H. J., & Koo, W. (2023). Analysis of various algorithms for optimizing the wave energy converters associated with a sloped wall-type breakwater. *Ocean Engineering*, *276*, 114199. https://doi.org/10.1016/j.oceaneng.2023.114199

Jeong, J. H., Kim, J. H., & Lee, J. L. (2021). Analysis of wave transmission characteristics on the TTP submerged breakwater using a parabolic-type linear wave deformation model. *Journal of Ocean Engineering and Technology*, *35*(1), 82−90. https://doi.org/10.26748/KSOE.2020.066

Jiang, L., Zhang, J., Tong, L., Guo, Y., He, R., & Sun, K. (2022). Wave motion and seabed response around a vertical structure sheltered by submerged breakwaters with Fabry−Pérot resonance. *Journal of Marine Science and Engineering*, *10*(11), 1797. https://doi.org/10.3390/jmse10111797

Kaveh, M., & Mesgari, M. S. (2023). Application of meta-heuristic algorithms for training neural networks and deep learning architectures: A comprehensive review. *Neural Processing Letters*, *55*(4), 4519−4622. https://doi.org/10.1007/s11063-022-11055-6

Khan, M. B., Behera, H., Sahoo, T., & Neelamani, S. (2021). Boundary element method for wave trapping by a multi-layered trapezoidal breakwater near a sloping rigid wall. *Meccanica*, *56*, 317−334. https://doi.org/10.1007/s11012-020-01286-z

Koley, S., Panduranga, K., Almashan, N., Neelamani, S., & Al-Ragum, A. (2020). Numerical and experimental modeling of water wave interaction with rubble mound offshore porous breakwaters. *Ocean Engineering*, *218*, 108218. https://doi.org/10.1016/j.oceaneng.2020.108218

Lamas-Pardo, M., Iglesias, G., & Carral, L. (2015). A review of very large floating structures (VLFS) for coastal and offshore uses. *Ocean Engineering*, *109*, 677−690. https://doi.org/10.1016/j.oceaneng.2015.09.012

Lee, W. D., Jeong, Y. M., & Hur, D. S. (2019). Wave control by tide-adapting submerged breakwater. *Journal of Ocean Engineering and Technology*, *33*(6), 573−580. https://doi.org/10.26748/KSOE.2019.081

Lee, J., Jeong, Y. M., Kim, J. S., & Hur, D. S. (2022). Analysis of hydraulic characteristics according to the cross-section changes in submerged rigid vegetation. *Journal of Ocean Engineering and Technology*, *36*(5), 326−339. https://doi.org/10.26748/KSOE.2022.028

Loukili, M., Dutykh, D., Nadjib, C., Ning, D., & Kotrasova, K. (2021). Analytical and numerical investigations applied to study the reflections and transmissions of a rectangular breakwater placed at the bottom of a wave tank. *Geosciences*, *11*(10), 430. https://doi.org/10.3390/geosciences11100430

Manisha, Kaligatla, R. B., & Sahoo, T. (2019). Effect of bottom undulation for mitigating wave-induced forces on a floating bridge. *Wave Motion*, *89*, 166−184. https://doi.org/10.1016/j.wavemoti.2019.03.007

Min, E. H., Koo, W., & Kim, M. H. (2023). Wave characteristics over a dual porous submerged breakwater using a fully nonlinear numerical wave tank with a porous domain. *Journal of Marine Science and Engineering*, *11*(9), 1648. https://doi.org/10.3390/jmse11091648

Ni, Y. L., & Teng, B. (2021a). Bragg resonant reflection of water waves by a Bragg breakwater with porous rectangular bars on a sloping permeable seabed. *Ocean Engineering*, *235*, 109333. https://doi.org/10.1016/j.oceaneng.2021.109333

Ni, Y. L., & Teng, B. (2021b). Bragg resonant reflection of water waves by a Bragg breakwater with porous trapezoidal bars on a sloping permeable seabed. *Applied Ocean Research*, *114*, 102770. https://doi.org/10.1016/j.apor.2021.102770

Patil, S. B., & Karmakar, D. (2021). Performance evaluation of submerged breakwater using multi-domain boundary element method. *Applied Ocean Research*, *114*, 102760. https://doi.org/10.1016/j.apor.2021.102760

Shi, Y., & Eberhart, R. C. (1998). Parameter selection in particle swarm optimization. In Porto, V.W., Saravanan, N., Waagen, D., & Eiben, A.E. (Eds.), *Evolutionary Programming VII. EP 1998. Lecture Notes in Computer Science, Vol. 1447*. (pp. 591−600). Springe. https://doi.org/10.1007/BFb00408

Tavana, H., & Khanjani, M. J. (2013). Reducing hydroelastic response of very large floating structure: a literature review. *International Journal of Computer Applications*, *71*(5), 13−17.

Vijay, K. G., Venkateswarlu, V., & Sahoo, T. (2021). Bragg scattering of surface gravity waves by an array of submerged breakwaters and a floating dock. *Wave Motion*, 106, 102807. https://doi.org/10.1016/j.wavemoti.2021.102807

Wang, C. M., Tay, Z. Y., Takagi, K., & Utsunomiya, T. (2010). Literature review of methods for mitigating hydroelastic response of VLFS under wave action. *Applied Mechanics Reviews*, *63*(3), 030802. https://doi.org/10.1115/1.4001690

Watanabe, E., Wang, C. M., Utsunomiya, T., & Moan, T. (2004). Very large floating structures: applications, analysis and design (Report No. 2004-02). *CORE Report*, 2, 104−109.

Zhang, P., Li, Y., Tang, Y., Zhang, R., Li, H., & Gu, J. (2023). Multi-objective optimization and dynamic response predictions of an articulated offshore wind turbine. *Ocean Engineering*, *273*, 114017. https://doi.org/10.1016/j.oceaneng.2023.114017

Zhu, K., Shi, H., Han, M., & Cao, F. (2022). Layout study of wave energy converter arrays by an artificial neural network and adaptive genetic algorithm. *Ocean Engineering*, *260*, 112072. https://doi.org/10.1016/j.oceaneng.2022.112072

Author ORCIDs

Author name	ORCID
Heo, Sanghwan	0000-0003-0033-5022
Koo, Weoncheol	0000-0002-4384-0996
Kim, Moo-Hyun	0000-0001-5793-3707